Supporting Information

Ag/ZnO microcavities with high sensitivity and self-cleaning properties for fast repetitive SERS detection

Jiale Zheng[a], Dongliang Liu[b], Xilong Liu[a], Zekai Wang[a], Junfeng Li[a], Xinxin Wang[a], Jun Wang[b], Qiang Fu[c], Yanqiang Cao[a], Liyong Jiang[a], Yikai Chen[a,d,*]

[a]School of Physics, Nanjing University of Science and Technology, Nanjing, 210094, China
[b]School of Science, Xi'an Polytechnic University, 19 Jinhua South Road, Xi'an 710048, China
[c]Department of Optoelectronic Information Science and Engineering, School of Physics and Materials Engineering, Hefei Normal University, Hefei 230601, China
[d]MIIT Key Laboratory of Semiconductor Microstructure and Quantum Sensing, Nanjing, 210094, China

[*]E-mail: ykchen@njust.edu.cn

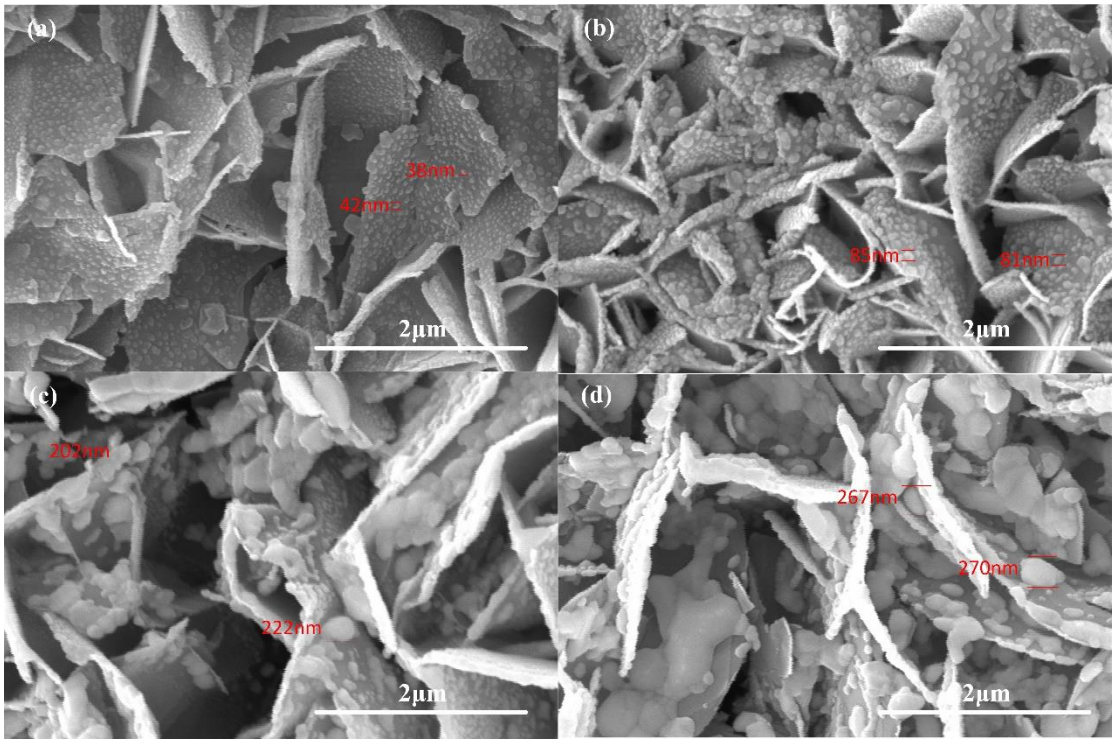

Fig. S1 SEM images of samples with different silver particle sizes

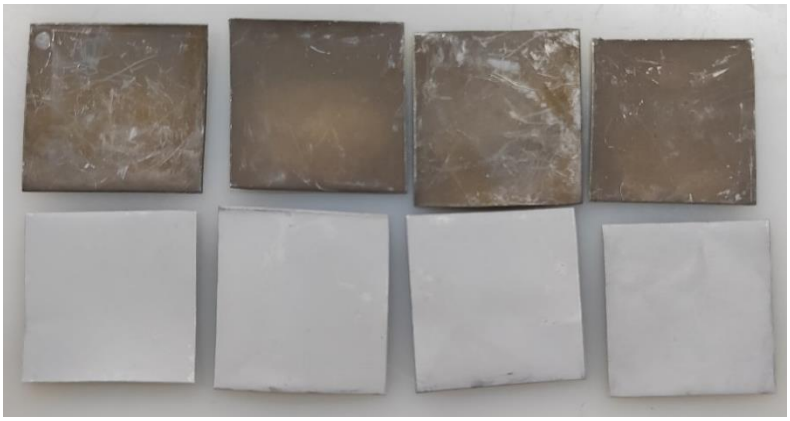

Fig. S2 Photos of the substrate

We control the particle size on the zinc oxide sample by changing different evaporation times. During the evaporation process, we also placed a blank glass substrate next to the sample as a control. Due to the large specific surface area of the micro cavities on the substrate surface, the deposition rate of silver is much lower than that of glass, and it is not easy to form a dense film. When the thickness of the silver film on the glass slide is about 25nm, the particles begin to grow and hardly form any particles. When the thickness of the silver film on the glass slide gradually increases to 33nm, 40nm, 48nm, and 55nm, the silver particles on the substrate correspond to Figure S1 (a) - (d), respectively. Figures from (a) - (d) clearly show the process of silver particles increasing from small to large and from thin to dense as the evaporation time increases. The size of the silver particles in Figure S1 (a) is mostly 30-40nm, at which point the silver particles have not yet begun to accumulate in large quantities and the

particle spacing is relatively large. In figure S1 (b), the number of silver particles is large, with a size of approximately 80-90nm. At this time, the ZnO are almost covered by silver particles and distributed evenly. In Figure S1(c), the size of the silver particles reaches 200nm, and the silver particles exhibit obvious aggregation and accumulation phenomena. In Figure S1 (d), the silver particles almost completely aggregate and many large connecting particles appear, with some silver particles reaching a size of 270nm. We selected the sample with the best enhancement effect, where the size of particles are approximately 80nm, for the experiment, shown in Figure S2.

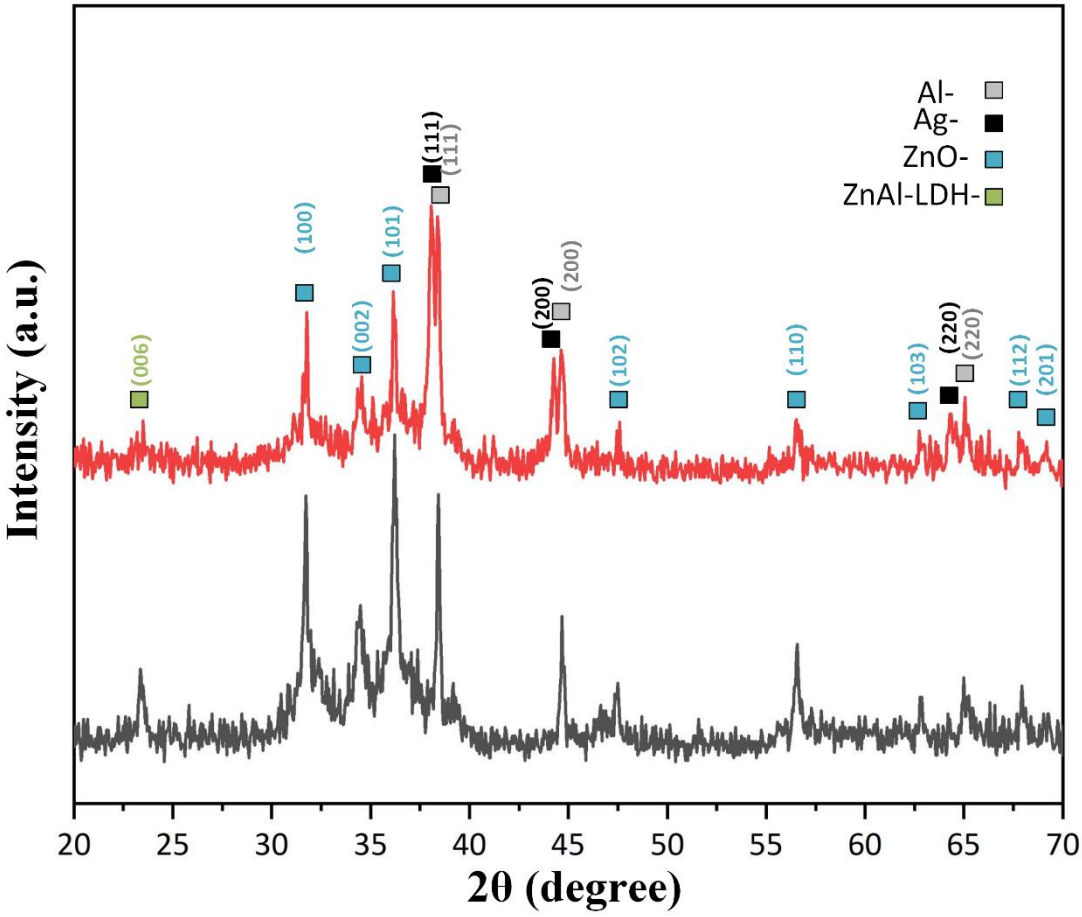

Fig. S3. The X-Ray Diffraction (XRD) for Ag/ZnO microcavities structures (red) and zinc oxide microcavities (gray).

The results from X-ray diffractometer (D8ADVACE, BRUKER) confirmed that the composition of the microcavity is zinc oxide, while the attached particles are silver. From Figure S3, eight blue marked diffraction peaks of pure ZnO can be observed, which correspond to the (100), (002), (101), (102), (110), (103), (112), and (201) crystal planes of ZnO with a hexagonal diamond structure. The three diffraction peaks of silver NP are located at 38.1°, 44.6°, and 64.3°, belong to the (111), (200), and (220) crystal planes of silver, respectively. The gray marked peak comes from the aluminum substrate. In addition, ZnAl-LDH is present during the one-step method, which is marked in green at 23.6°, corresponding to the (006) crystal plane of ZnAl-LDH.

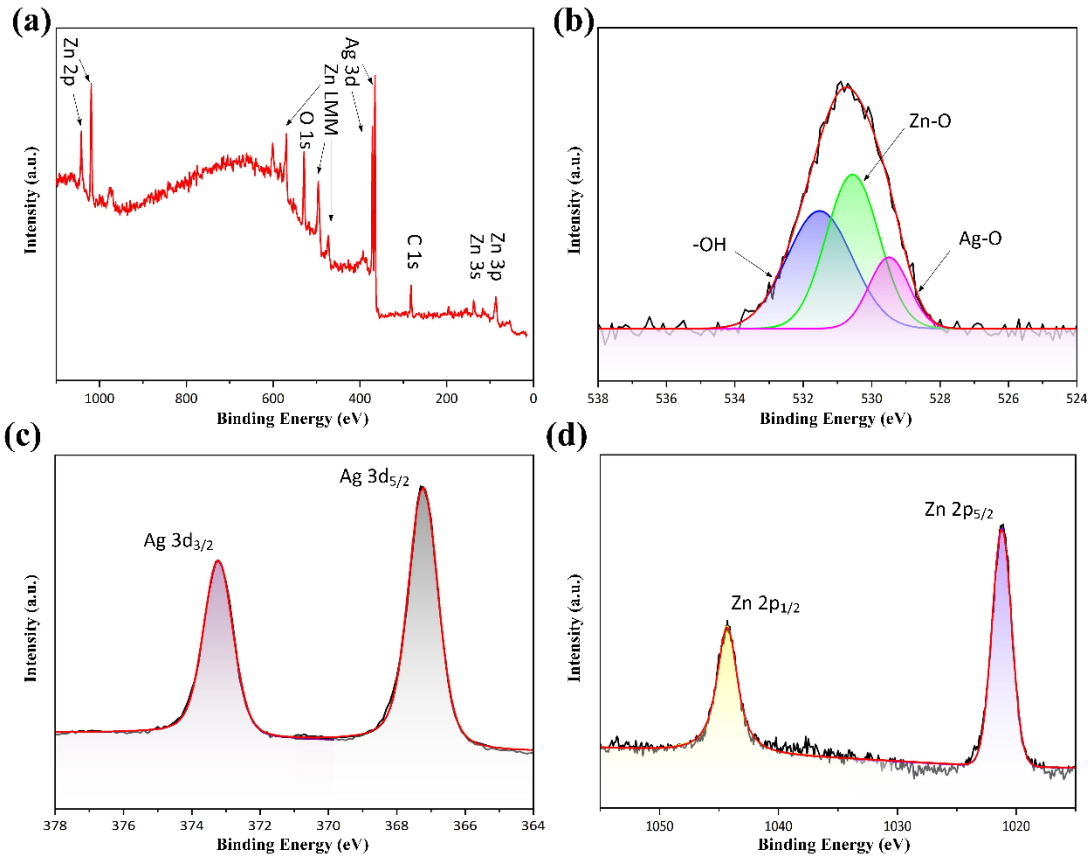

Fig. S4. (a) XPS spectrum of the Ag/ZnO microcavities structures. High-resolution spectra of (b) O 1s, (c) Ag 3d, and (d) Zn 2p, respectively.

The fully automated focus scanning micro-area X-ray photoelectron spectrometer (PHI Quantra lI) has been used to measure the XPS spectrum of the sample, proving the formation of the heterogeneous structure of Ag@ZnO. From the Figure S4 (a), Zn, O, and Ag elements are clearly detected. Through the high-resolution spectroscopy of O 1s, three different types of O can be observed. The peaks at 529.5 eV, 530.2, and 531.6 eV are silver oxide lattice oxygen, zinc oxide lattice oxygen, and chemisorbed oxygen produced by silver particle oxidation, respectively, shown as Figure S4(b). Combined with Figure S4 (c), it can be confirmed that Ag exists and some silver particles are oxidized, which proves that the enhancement effect of our chip still has the possibility of further improvement. Finally, as shown in Figure S4 (d), it is also confirmed that the binding energy of 1044.6 and 1021.4 eV can be attributed to Zn 2p1/2 and 2p3/2, derived from divalent zinc ions in zinc oxide.

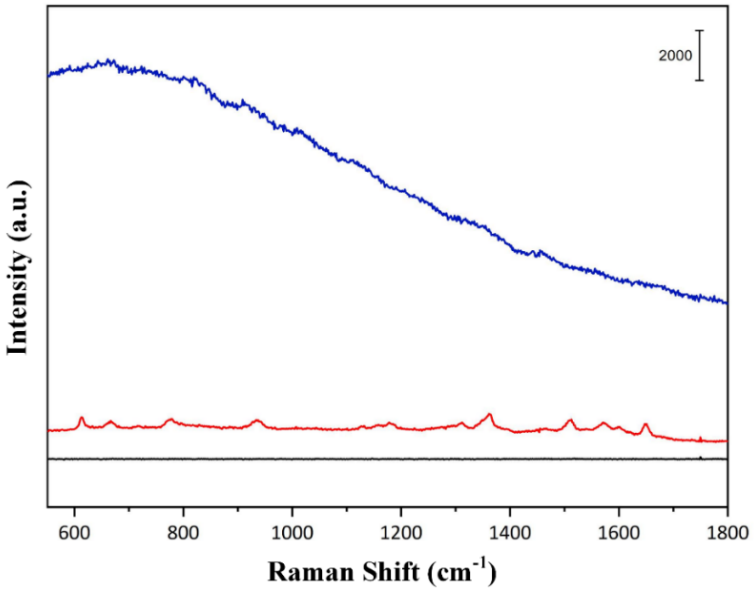

Fig. S5. The Raman spectrum of the R6G (10^{-9}M) on the Ag/ZnO microcavities (red), an aluminum foil coated with zinc oxide (blue) and the silver film (40nm) (black)

The comparison shows that combining silver particles and zinc oxide can greatly enhance the surface-enhanced Raman performance, much more than the zinc oxide structure and silver particles alone.

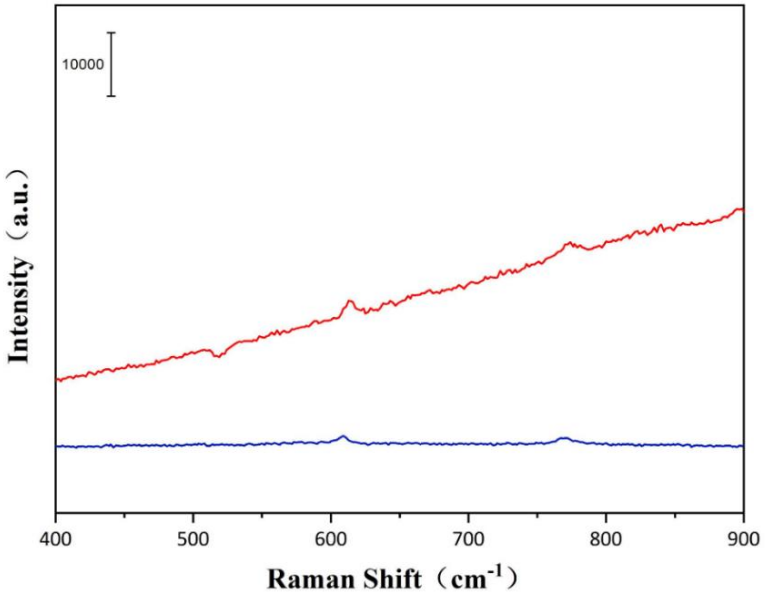

Fig. S6. The Raman spectrum of the R6G (10^{-3}M) on an aluminum foil (red) and the Raman spectrum of the R6G (10^{-11}M) on Ag/ZnO microcavities (blue).

The combination of the EF calculation formula and the SERS detection spectra can be extrapolated to the EF of a sample when the silver particles are around 80nm.

$$EF = \frac{I_{SERS} / N_{SERS}}{I_{Ref} / N_{Ref}} = 2.6 \times 10^{7}$$

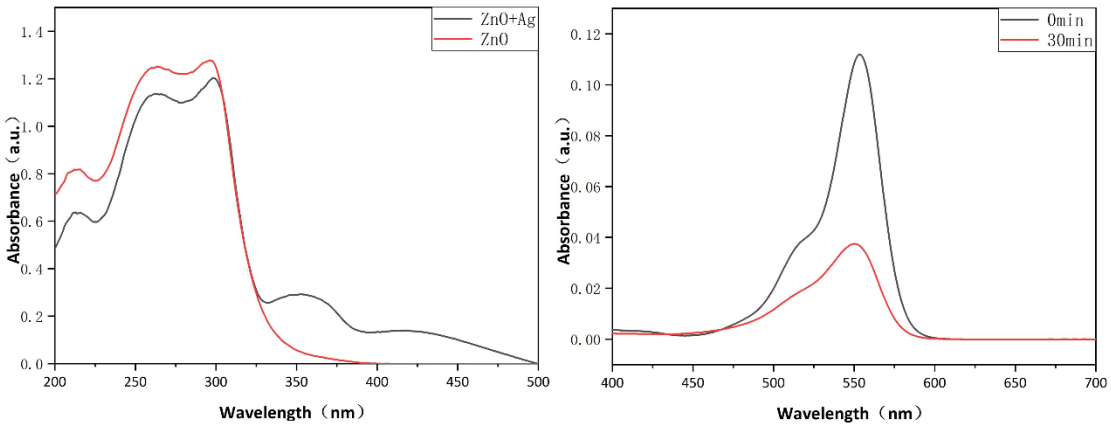

Fig. S7. (a) The UV absorption spectrum of Ag/ZnO microcavities (black solid line), and the Zn substrate as control group (red solid line). (b)The UV absorption spectrum of Rhodamine B (RhB) solution with Ag/ZnO microcavities substrate before (black solid line) and after (red solid line) 30 minutes irradiation by white light.

From the absorption spectrum (UV-Vis Spectrophotometer, UV-2600i, Shimadzu) of the substrate, it can be seen from Figure S7 (a) that the zinc oxide microcavities have extremely strong absorption in the wavelength range from 200 to 330nm, while the addition of silver particles widens the absorption wavelength of the substrate. Then, the above substrate was placed in RhB solution (20mg/L) and the absorption spectrum of the solution was measured after being irradiated with white light for 30 minutes, shown as the red solid line in Figure S7 (b). Compared with the absorption spectrum of RhB before irradiation (the black solid line), it degrade about 66% of RhB within 30 minute, which, therefore, also proves that the substrate has photocatalytic ability.

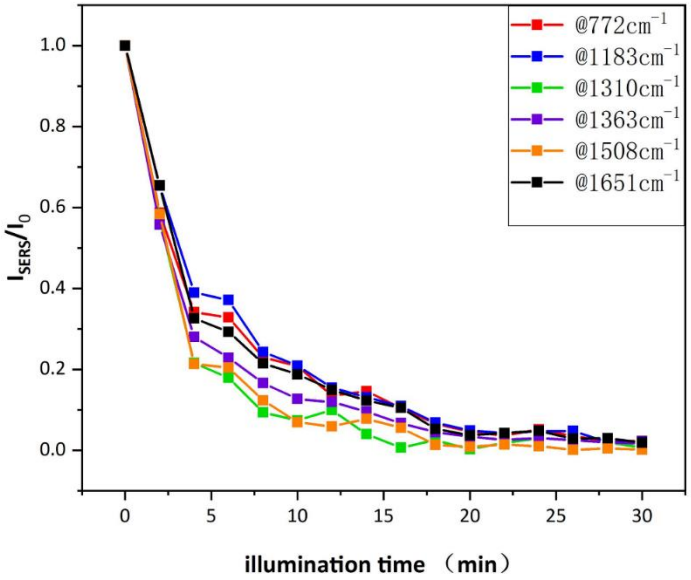

Fig. S8. The Intensity variation of a Raman signal @772cm^{-1}, @1183cm^{-1}, @1310cm^{-1}, @1363cm^{-1}, @1508cm^{-1}, @1651cm^{-1} over time within one cycle.

The Raman signals generated by the respiratory vibration of the benzene ring in

the R6G molecule were quantitatively analyzed, as shown in the above Figure S8. The intensities of the Raman characteristic peaks of R6Gs decayed exponentially with the irradiation time of the UV lamp. The intensity of the Raman signal decreased to about 55% of the initial value after two minutes of irradiation, and the molecule was virtually absent after 30 minutes, which means that the substrate can clean Rhodamine 6G (10^{-7}M) under irradiation.

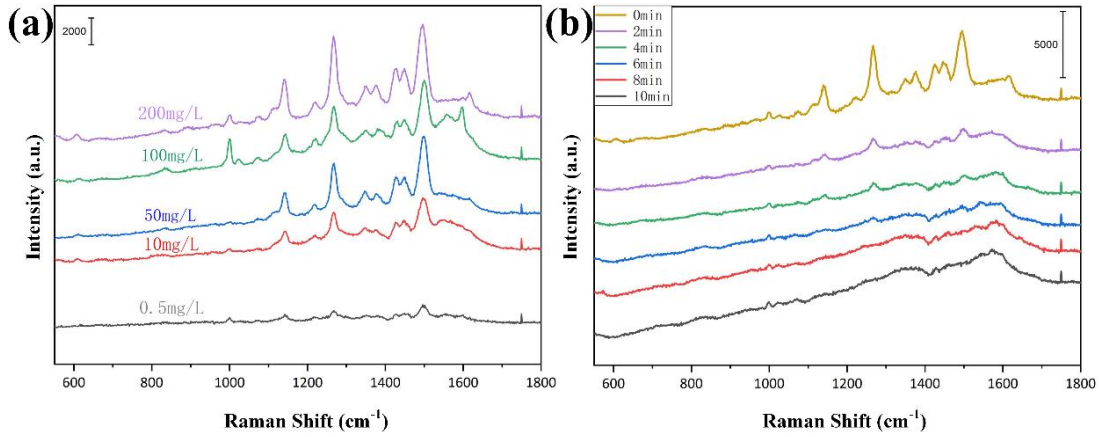

Fig. S9. (a) Raman spectra of sodium benzoate (0.5mg/L-200mg/L) on the optimized substrate. (b) The Raman spectrum of sodium benzoate (200mg/L) during irradiation.

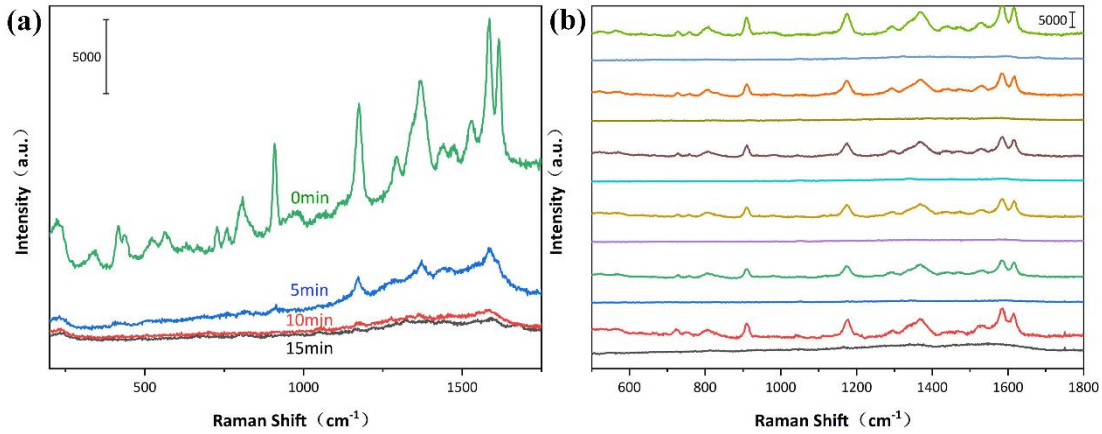

Fig. S10. (a) The Raman spectrum of 4-Mercaptobenzoic acid (4-MBA, 10^{-4}M) during irradiation. (b) Repeated Raman spectra after self-cleaning

Different concentration gradients were examined using sodium benzoate as a probe molecule and the ability to decompose was preliminarily explored in Figure S9. In addition, we used 4-MBA as a probe molecule to test the self-cleaning performance. As shown in Figure S10 (a), the Raman spectral decreases rapidly with the prolongation of irradiation, and almost disappears finally at 15 minutes, which means the 4-MBA on the substrate has been effectively decomposed. To further verify that the substrate still has the ability to enhance the electric field after molecular decomposition, the substrate was reused in situ to measure the Raman spectra of another prepared 4-MBA solution. After five repeated test, the substrate still maintained a very high and stable SERS enhancement, shown in Figure S10 (b).Therefore, the reusability of this SERS substrate has potential applications in the food safety and pharmaceutical industries.